Performance Enhancement of a Vertical Tail Model with Sweeping Jet Actuators

Roman Seele[*], Emilio Graff[†]
California Institute of Technology, Pasadena, CA, 91125, USA

John Lin[‡]
NASA Langley Research Center, Hampton, Virginia, 23681, USA

Israel Wygnanski[§]
The University of Arizona, Tucson, AZ, 85721, USA

Active Flow Control (AFC) experiments performed at the Caltech Lucas Adaptive Wall Wind Tunnel on a 12%-thick, generic vertical tail model indicated that sweeping jets emanating from the trailing edge (TE) of the vertical stabilizer significantly increased the side force coefficient for a wide range of rudder deflection angles and yaw angles at free-stream velocities approaching takeoff rotation speed. The results indicated that 2% blowing momentum coefficient (C_μ) increased the side force in excess of 50% at the maximum conventional rudder deflection angle in the absence of yaw. Even $C_\mu = 0.5\%$ increased the side force in excess of 20% under these conditions. This effort was sponsored by the NASA Environmentally Responsible Aviation (ERA) project and the successful demonstration of this flow-control application could have far reaching implications. It could lead to effective applications of AFC technologies on key aircraft control surfaces and lift enhancing devices (flaps) that would aid in reduction of fuel consumption through a decrease in size and weight of wings and control surfaces or a reduction of the noise footprint due to steeper climb and descent.

Nomenclature

β:　Angle of incidence
δ_R:　Rudder deflection angle [normalized by arbitrary maximal value]
ρ_∞:　Free stream density
Λ:　Sweep back angle
AFC: Active Flow Control
A_{nozzle}: Total area of all active nozzle exits
A_{ref}: Total projected area of the entire vertical stabilizer model
b:　total span width
c:　total local chord length
C_{Yn}: Normalized side force coefficient relative to baseline of δ_R=60% and β=0°
C_{Dn}: Normalized drag coefficient relative to baseline of δ_R=60% and β=0°
C_P: Pressure coefficient
C_Q: Mass flow coefficient, $\quad \frac{Q}{A_{ref}*u_\infty}$
C_μ: Momentum coefficient, $\quad \frac{J}{0.5*A_{ref}*\rho_\infty*u_\infty^2} = 2\frac{A_{nozzle}}{A_{ref}}*\left(\frac{u_j}{u_\infty}\right)^2$
J:　Jet (or actuation) momentum
LE:　Leading edge

---

[*] Research Associate, Graduate Aerospace Laboratories, seele@caltech.edu
[†] Research Project Manager, Graduate Aerospace Laboratories
[‡] Senior Scientist, Flow Physics and Controls Branch, AIAA Associate Fellow
[§] Professor, Aerospace and Mechanical Engineering Department, AIAA Fellow

1

M: Mach number
MAC: Mean aerodynamic chord
p_{ch}:   pressure in the settling chamber upstream of the actuators
Q: Actual volume flow rate of actuation
Re: Reynolds number based on MAC
Sp: Spanwise distance between adjacent actuators [in]
TE: Trailing edge
U_c: Speed of sound ≈ 1116ft/s (≈ 340m/s)
u_j: Theoretical jet velocity of the sweeping jet at the nozzle
u_∞:   Free stream velocity
x':   Direction perpendicular to the LE of the vertical stabilizer and the rudder respectively
x: Streamwise direction (parallel to free stream)
z: Spanwise direction (perpendicular to free stream and tunnel floor)

I.   Introduction

The size of the vertical tail on a commercial airliner is determined by the eventuality of losing an engine during takeoff and low speed climb (see Fig. 1). It is a large surface that is hardly used under normal flight conditions although it is indispensible during "engine out" emergency and it is needed during crosswind takeoff and landing. In addition, the vertical tails usually sized for the shortest version in an aircraft's model family (see an example in Fig. 2a), which made them somewhat oversized for the longer versions in the family. The safe landing of the tailless B-52 shown in Fig. 2b attests to some of its redundancy in non-critical situations. Although seldom used to its full capability, its presence adds drag and weight to the aircraft thus increasing fuel consumption. Active flow control devices that delay flow separation over a highly deflected rudder may enable a smaller vertical tail to provide the control authority needed during emergency, resulting in weight and drag reduction as well as fuel savings. These benefits are of significant interest for the NASA ERA project. The present experiment was initiated to establish the efficacy of such system.

The capabilities of Active Flow Control have been demonstrated on airplane and component models in laboratory environment. In few instances they were demonstrated in flight and in some cases they were actually used on military airplanes but they were not incorporated into a commercial airliner. The reasons given are many but the popular beliefs focus on the complexity, reliability and weight of the actuation system and on its appetite for power.
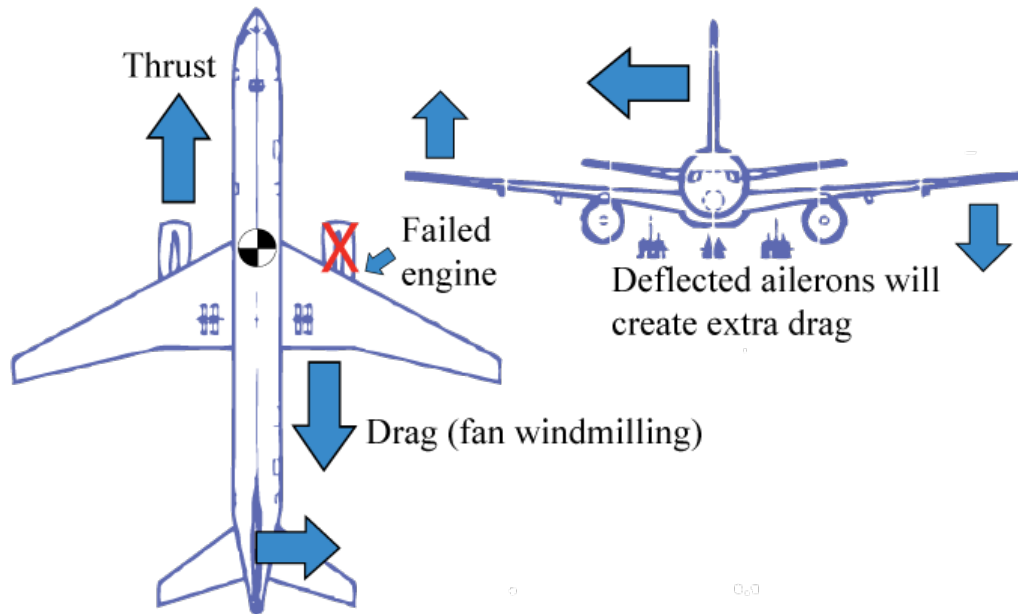

Fig. 1 Necessary trim settings of an airplane in case of engine failure
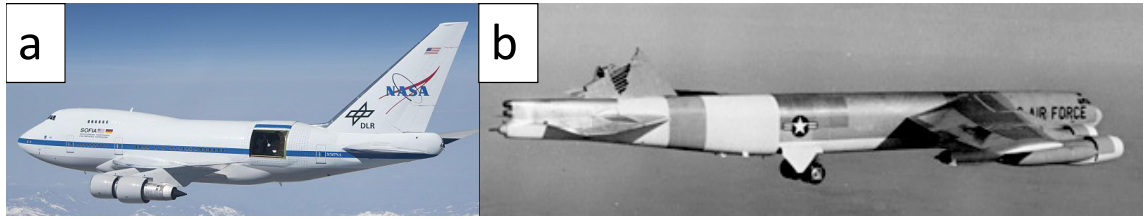
Fig. 2 (a) Short body version of a 747, credit: NASA/ Jim Ross; (b) A B-52H that lost its vertical tail in clear air turbulence, credit: Wikipedia/ United States Air Force

Various actuation methods have been researched [1] and have shown different degrees of effectiveness. Sweeping jet actuators are attractive because they have no moving parts, but they do require a steady supply of compressed air. In this sense they resemble steady blowing although they use less air. A schematic drawing of a typical actuator is shown in Fig. 3. It emits a continuous jet that flips from one side of the outlet nozzle to the other. The air passing through the entrance nozzle on the left of Fig. 3 attaches itself to one of the solid surfaces forming the walls of the main cavity of the actuator e.g. in the case shown it is attached to the upper surface. The jet curves as it rushes to the outlet increasing the pressure at the inlet to the upper feedback channel. This creates flow in the feedback channel that pushes the entering jet back to the opposite surface and repeats the process. Two Schlieren photographs are also shown in Fig. 3 demonstrating the sweeping process when the exit jet velocity is supersonic. The oscillation is therefore two-dimensional in nature although the jet is three-dimensional and can be inclined to the downstream surface of the wing at any angle. Its frequency is determined by its dimensions (mostly the length of the feedback channel), but its spanwise sweep angle depends on the detailed design of the actuator. In some of those designs [2 - 4] a wedge was placed in the center of the exit nozzle to ensure that the resulting oscillatory jet dwells at two prescribed angles. The actuator does not have to be curved as the one shown in Fig. 3, in fact many previous experiments were carried out using rectangular actuators as described by Lucas et al. [5].
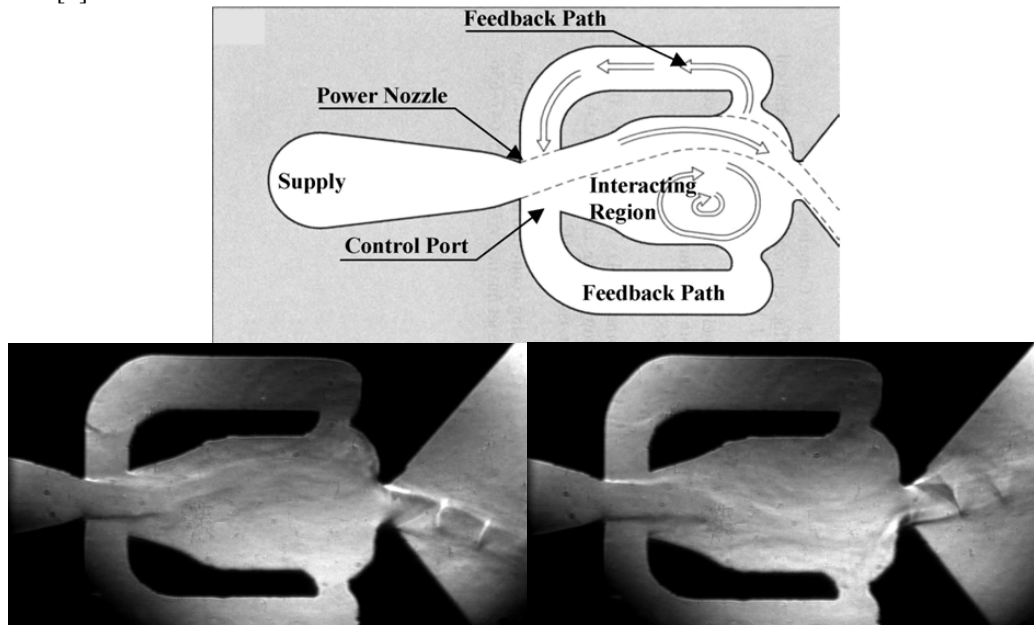

Fig. 3 Conceptual design of sweeping jet actuator [13] and visualization of its sweeping motion when the exit jet is supersonic

The sweeping jet actuators have been developed more than fifty years ago at the Harry Diamond Research Laboratories where they were initially considered for use in analog computers and as fluidic amplifiers. For years they have been mostly used as oscillating windshield washers on cars, showerheads

3

and irrigation systems using liquid, mostly water, as the working fluid. Recently, these devices were used in aeronautical experiments for the purpose of delaying separation on airfoils [6-8] and on wings [9]. The usefulness of these devices prompted the need to understand how they work [10] and their effect on boundary layers that are about to separate from the surface. In the interim one may improve the efficiency of these actuators for a specific application by using dimensional analysis that enables one to determine the leading parameters controlling the process [11, 12] and this is approximately the manner in which they were applied presently.

In this experiment we follow the path of Rathay et al. [14, 15] who applied synthetic jet actuators to a typical vertical stabilizer of a commercial airplane model. Their actuators were placed in a linear array next to the hinge of the rudder for the purpose of attaching the flow over the rudder surface at large rudder deflection angles, thereby increasing its effectiveness. An earlier paper [16] focused on sweeping jet actuation that was applied directly to the rudder, while this paper mostly discusses the effects of actuation that is applied from the trailing edge of the main element. Applying sweeping jet AFC on the trailing edge of the vertical stabilizer does have a potential advantage over the rudder location from a system integration perspective as it avoids dealing with moving components.

II.   Experimental Setup and Instrumentation

The vertical stabilizer model has a NACA 0012 shape and was designed based on publicly available information and tested at the California Institute of Technology's Lucas Wind Tunnel [17], as shown in Fig. 4. The wing is tapered and swept back by Λ=42° at the leading edge (LE), has a 35% chord flap, a 1.765ft (0.538m) MAC, a span b=3.5ft (1.067m) and features a dorsal fin similar to what is used on a real stabilizer to smoothen the transition between fuselage and stabilizer. The closed loop wind tunnel's test section is 6ft (1.828m) high and 5ft (1.524m) wide and is operated at speeds of up to 50m/s for this experiment. A ground plane that houses a six component strain gage balance was used to support the model through a strake. This ground plane decreased the effective height of the wind tunnel to 4.25ft (1.295m). Since the walls of the tunnel can be deflected, they were set to offset the effect of the ground plane. A fairing that roughly approximates the shape of the fuselage was installed around the model and attached to the ground plane to minimize the effect of the developing boundary layer at the wall. To minimize Reynolds number and transition related effects tripping dots were applied at x'/c=5% on the models suction side and at x'/c=10% on the pressure side.
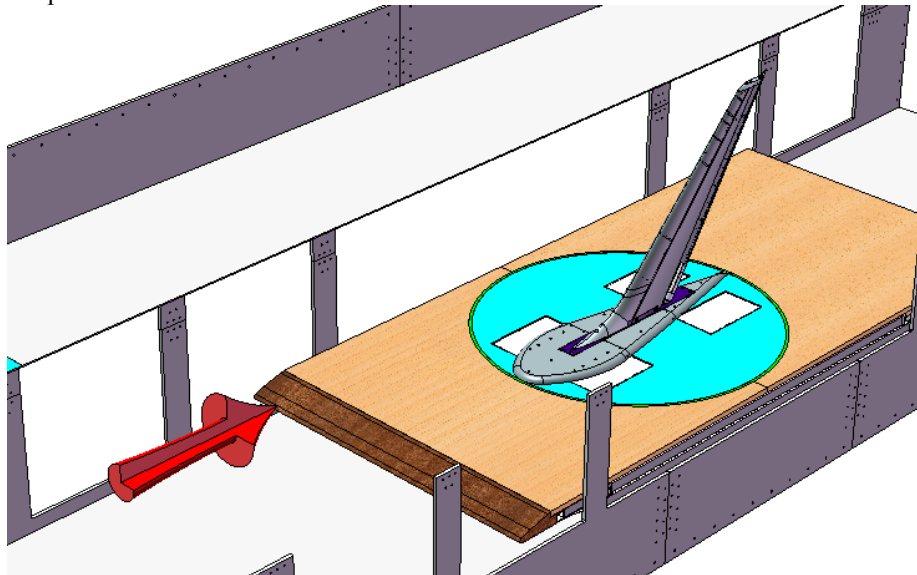

Fig. 4 Vertical stabilizer setup in the Lucas Wind Tunnel test section

Pressure distributions at various spanwise and chordwise locations were evaluated with a Pressure Systems, Inc. 8400 system. The stabilizer is equipped with roughly 230 static pressure ports arranged in a spanwise and chordwise grid oriented relative to the LE of the main element and the rudder. The three

major chordwise rows feature between 36 and 39 static pressure ports and are located at z/b=40%, 70% and 89% relative to their starting point at the LE of the model (Fig. 5). A number of additional ports are used to assess the flow in spanwise direction.
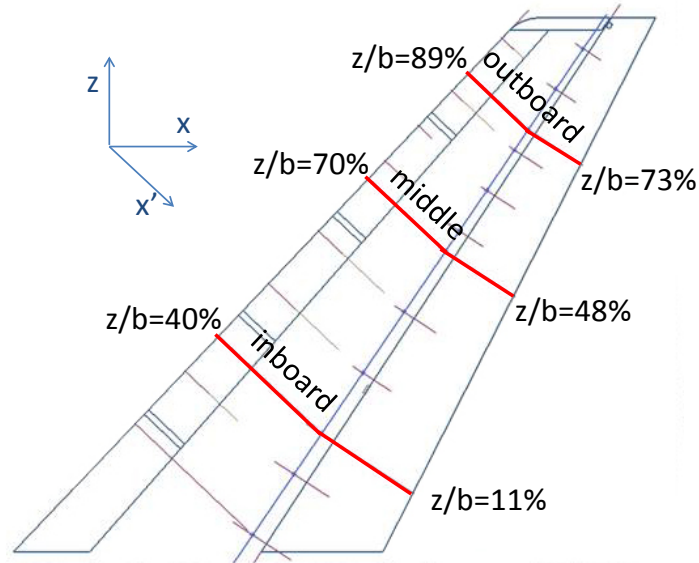

Fig. 5 Position of chordwise pressure tap rows (shown without dorsal fin)

The sweeping jet actuators were supplied with compressed air through the root of the model. Hose forces were assessed in various different arrangements and found to exert negligible loads on the model. The air supply was controlled by an electronic pressure regulator while the ejected mass flow was recorded by a flow meter with analog output and digitally corrected for pressure and temperature. All 32 actuators are located at the trailing edge of the main element. The ejection angle relative to the surface is roughly 10° and the narrowest achievable spacing on the rudder is 0.5in. (12.7mm). Actuators can be blocked individually thereby achieving different spatial actuator distributions.

III.   Results

A. General efficiency of AFC from the TE
The side force generated by a conventional rudder at small deflection angles, δ_R (the parameter is normalized by an arbitrary maximum value), is linearly proportional to δ_R prior to the occurrence of separation. An increase of rudder deflection beyond the δ_R corresponding to the initiation of separation thus results in reduced rudder effectiveness noticed by a reduction in $dC_{Yn}/d\delta_R$ (Fig. 6a) and a concomitant increase in drag. For the present rudder-tail configuration the initial signs of reduced effectiveness already occur at δ_R>20% and it becomes more pronounced at δ_R>60% which most likely determines the maximum effective rudder deflection for a given configuration. Thus the need for a prescribed side force at different stages of the flight envelope determines the size of the rudder and the vertical tail. Sweeping jet actuation at C_μ=0.5% maintains a constant $(dC_{Yn}/d\delta_R)$ up to $\delta_R\approx$50% while it requires a C_μ=1.5% to increase the linear dependence of C_{Yn} up to δ_R=60%. At that point the side force coefficient C_{Yn} increases to 1.5 thus exceeding the side force generated by the vertical tail by 50%.

The jet momentum coefficient, C_μ, was used as the leading parameter affecting the state of the flow over the rudder because it is traditionally used whenever blowing is applied to control flow separation and circulation over wings. The length scales or area ratios used in the definition of C_μ may be unique for flapless airfoils but their uniqueness is lost when flaps and slats are introduced to airfoils and even more so for finite wings. In the case of a highly deflected rudder it may be the rudder area that determines the momentum required to control the flow and not the area of the entire vertical tail. The use of sweeping jets emanating from discrete sources provides additional length scales of significance e.g.: the size of the

5

actuators' nozzles and their aspect ratio as well as the distance between adjacent actuators. These and other parameters have to be carefully considered when contemplating application to a large airplane.
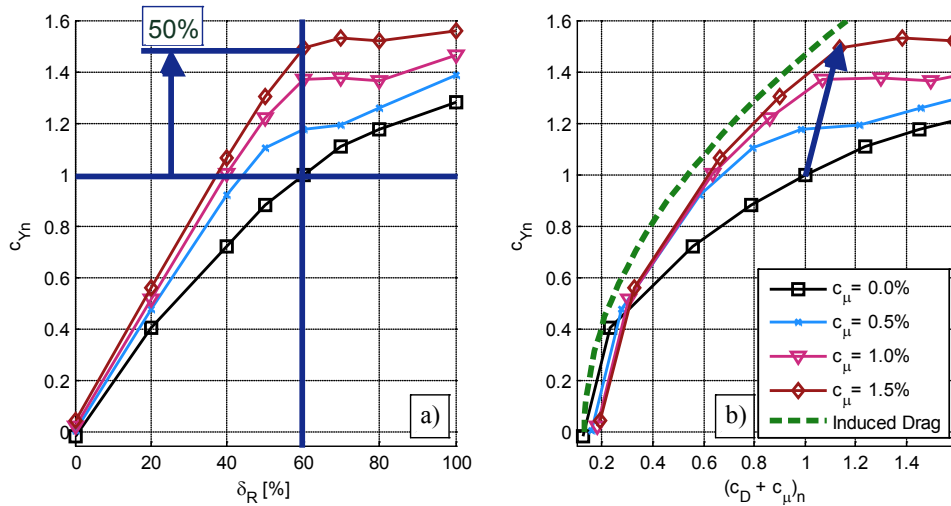

Fig. 6 Lift and drag polars for β=0° at u_∞=40m/s with 1.5in. spacing.

The increase in drag resulting from the use of sweeping jets at various rudder deflections is shown in Fig. 6b. The drag polars plotted in this figure presume that the entire jet momentum is recovered as thrust, thus the abscissa represents $(C_D + C_\mu)_n$ instead of the traditional C_D. The arrow originating at (1; 1) in this figure and pointing at (1.1; 1.5) represents the increase in $(C_D + C_\mu)_n$ due to 50% increase in side force by application of Active Flow Control (AFC) at δ_R=60%. This increase is attributed to the induced drag because of the increase in side force (lift). The dashed green line in Fig. 6b represents the increase in drag due to lift by assuming an elliptical load distribution on a wing having an aspect ratio that is twice the height of the vertical tail. The factor of two arises from the image representing the floor of the tunnel. It clearly predicts the increase in induced drag encountered, although the lift distribution on the vertical tail is not elliptical.
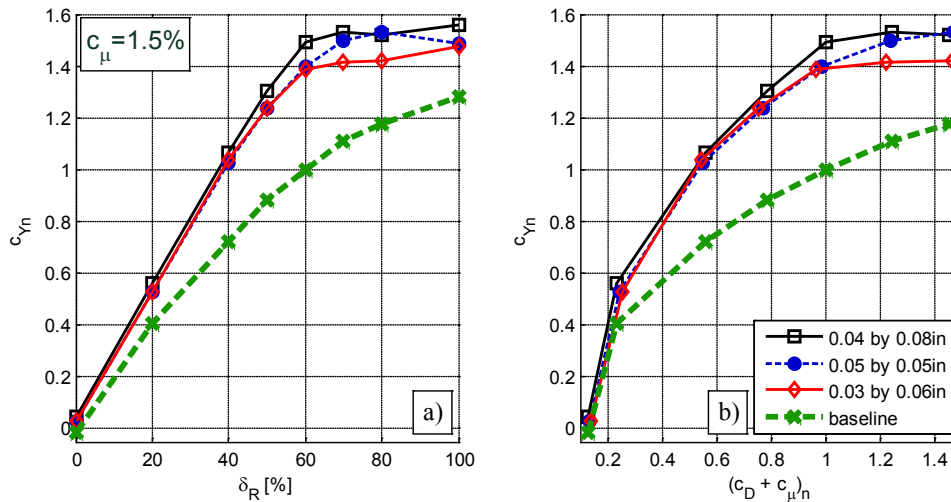

Fig. 7 Different actuator sizes at a fixed C_μ=1.5%, lift and drag polars for β=0° at u_∞=40m/s with 1.5in. spacing.

Reducing the size of the actuators while maintaining a constant C_μ=1.5% had a slightly deleterious effect on the C_{Yn} generated at a given δ_R>40% (Fig. 7a). In two of the cases compared, the aspect ratio of the exit nozzle was maintained but its size was halved. The deterioration in side force production is

6

attributed to the fact that the larger nozzle (0.04 by 0.08in.) chokes around $C_\mu \approx 1.8\%$ while the smaller nozzle (0.03 by 0.06in.) already attains supersonic speed for $C_\mu \approx 1.0\%$. Flow visualization (Fig. 3) suggests that the jet does not attach to the nozzles outside wall when the flow is supersonic. For $C_\mu = 1.5\%$ the exit velocity of the large nozzle is subsonic while it is supersonic for the smaller one (0.03 by 0.06in.). This may have contributed to the reduction in control authority. The flow from the intermediate nozzle (0.05 by 0.05in.) was also supersonic at that input level but the different throat aspect ratio may have enabled it to penetrate the separated boundary layer more effectively than the flatter nozzles could, thus improving its control authority for large rudder deflections (Fig. 7).
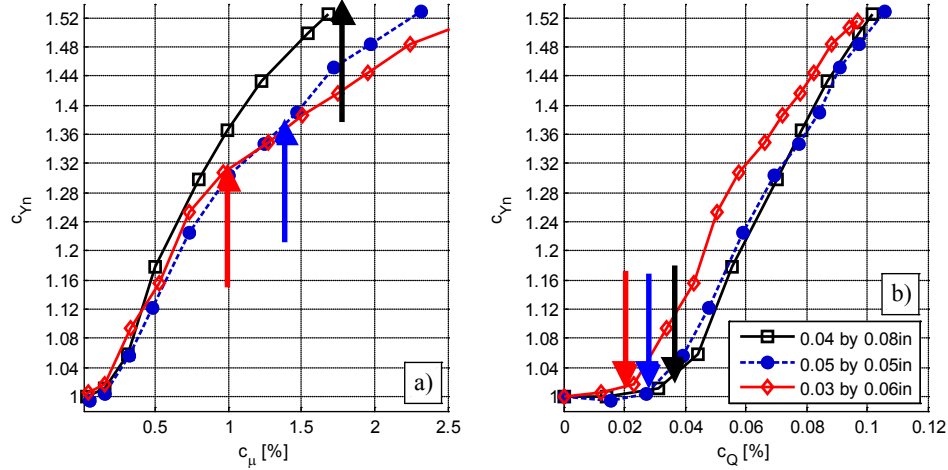

Fig. 8 Different actuator sizes, lift vs. momentum and mass flow for $\delta_R=60\%$, $\beta=0°$ at $u_\infty=40$m/s with 1.5in. spacing (arrows pointing up indicate $U_j=U_c$; arrows pointing down indicate $U_j=3\cdot U_\infty$).

One may fix the rudder deflection angle ($\delta_R=60\%$) and observe the effect of increasing C_μ on the increase in C_{Yn} for the three nozzles tested (Fig. 8). It appears that as long as the flow though the nozzles is subsonic, the C_{Yn} generated by AFC is not sensitive to the nozzle size or its throat aspect ratio. However, once the flow through the nozzle throat becomes supersonic, the slope of (dC_{Yn}/dC_μ) is lower due to the inhibited sweep angle of the sweeping jet. In Fig. 8a, the arrows pointing up indicate where U_j equals the speed of sound U_c. Thus compressibility affects the control authority of the sweeping jets. It is well known [18] that a steady supersonic jet has a lower spreading rate than a subsonic one (i.e. it is less effective at entraining ambient fluid than a subsonic jet of the same jet momentum) and the same seems to hold true for the sweeping jets. The dependence of the side force on C_Q is shown in Fig. 8b. It indicates that a threshold value of ($U_j = 3\cdot U_\infty$) is required before any benefits can be reaped from the sweeping jets. As long as U_j is of the same order as U_∞ and the flow is incompressible the volume flow emanating from the nozzle simply displaces the streamlines outward. When $U_j >> 3\cdot U_\infty$ and the jet is attached to the surface (wall jet), entrainment of ambient fluid bends the streamlines toward the surface thus enabling the flow to turn around the deflected rudder. The threshold C_Q is smallest for the smallest nozzle because U_j/U_∞ is the largest for a given jet volume flow. In terms of its effect on the outer potential flow, a slow jet may be represented by a point source while a fast one is a line sink whose local strength is diminishing along the path of the jet. Earlier studies [19] have shown that the most effective separation control by steady blowing occurs when the jet emanates from the narrowest slot placed near the natural separation location.

The mass flow supplied to the vertical tail and the pressure in the settling chamber leading to the sweeping jet actuators, can easily be measured. On the other hand, measuring the average jet velocity emanating from the actuators' nozzles requires extensive effort, or it can be calculated using crude one dimensional approximation. Thus instead of analyzing the data in terms of momentum one may define a power coefficient, C_π, that is dependent on the pressure in the settling chamber upstream of the actuators, p_{ch}, and the total mass flow Q:

$$c_\pi = \frac{Q * p_{ch}}{\frac{1}{2} * \rho_\infty * A_{ref} * u_\infty^3}$$
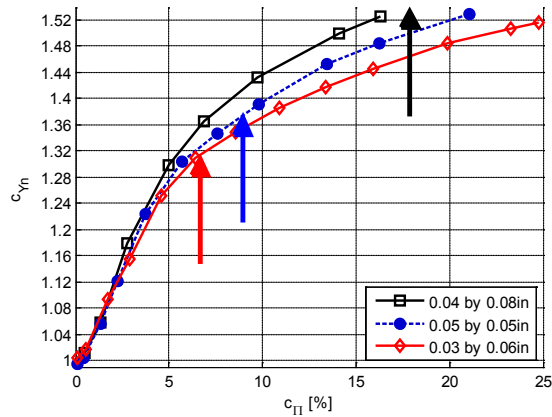
7

Fig. 9 Different actuator sizes, Lift vs. power for δ_R=60%, β=0° at u_∞=40m/s with Sp=1.5in., (arrows pointing up indicate U_j=U_c).

Since the volume flow multiplied with chamber pressure has the dimension of power it allows one to judge the efficiency of the actuation by the power a compressor or an electrical input provides in realistic applications. Thus, C_π establishes a simple factor by which actuation can be evaluated from an engineering perspective. While the results shown in Fig. 8b suggest that using smaller orifices consumes less mass flow to provide a given C_{Yn} increase, Fig. 9 indicates that it does so at a cost of higher power requirement C_π and a much higher p_{ch}. Both C_π and C_μ lead to similar conclusions suggesting that the larger 0.04 by 0.08 in. actuators perform more efficiently than the smaller ones because they do not choke at small values of C_μ.

The effects of actuator size on the side-force generated by the rudder, assuming that all actuators were identical and evenly distributed along the span, were discussed above. However, instead of changing the orifice size of the actuators one may change the distance between adjacent actuators, Sp. This gives one the ability to maintain a given average momentum at a given level of mass flow input thus exchanging Sp, with actuator size. Fig. 10 shows the effects of Sp on actuators with an orifice size of 0.04 by 0.08 in. and 0.03 by 0.06 in. at a prescribed δ_R=60%. For a given C_Q<0.08 increasing the distance between adjacent actuators increases the C_{Yn} generated by the rudder. At very low C_Q and increase in Sp implies a substantial increase in U_j that lowers the threshold of C_Q at which the jet starts entraining ambient fluid. By quintupling the distance between actuators to 7.5 in. (i.e. to Sp/MAC≈2.8) one may generate a 20% improvement in C_{Yn} at C_Q=0.015% or C_μ=0.2%. However, at higher C_μ the actuator nozzle chokes early and the slope (dC_{Yn}/dC_μ) rapidly decreases because the jets do not sweep as far as they did when they were still subsonic. As a result, when the jets are supersonic large areas between the actuators are left unexposed to the positive effects of actuation. Therefore, to achieve a desired improvement in C_{Yn} at a prescribed rudder deflection there is a confluence of geometrical parameters (i.e. actuator size and spacing) that are interchangeable. For example: to obtain a C_{Yn}=1.24 one may need a C_μ=0.5% and a C_Q=0.03% corresponding to actuator spacing of 4.5in.≤Sp≤7.5inches. One may also obtain a C_{Yn}=1.4 corresponding to C_Q≈0.08 at Sp=1.5in. or 3.0inch, but the difference in the momentum coefficient required is almost double. This is because the emanating jets corresponding to Sp=3inches are supersonic.

Comparing the results obtained with 0.04 by 0.08in. actuators with smaller ones having nozzle dimensions 0.03 by 0.06in. (or 56% of the area of the larger nozzles) shows the characteristics discussed more clearly. The threshold level of C_Q at which the sweeping jets became effective is lower and it scaled up approximately as the area ratio of the two sets of actuators. When the nozzles were spaced 1.5in. apart the flow through them chocked at C_μ≈1% which resulted in a substantially lower slope (dC_{Yn}/dC_μ) for C_μ>1% (Fig. 10c). It is interesting to note that using the smaller actuators requires a slightly higher C_μ to obtain a C_{Yn}=1.24 (i.e. C_μ≈0.7% for most actuators' spacings) but it requires a slightly lower C_Q to obtain C_{Yn}=1.4. More importantly the maximum C_{Yn}=1.53 attained using the larger actuators at C_μ=1.6% that was not attainable using the smaller ones at C_μ>2.5% (corresponding to a roughly identical C_Q).
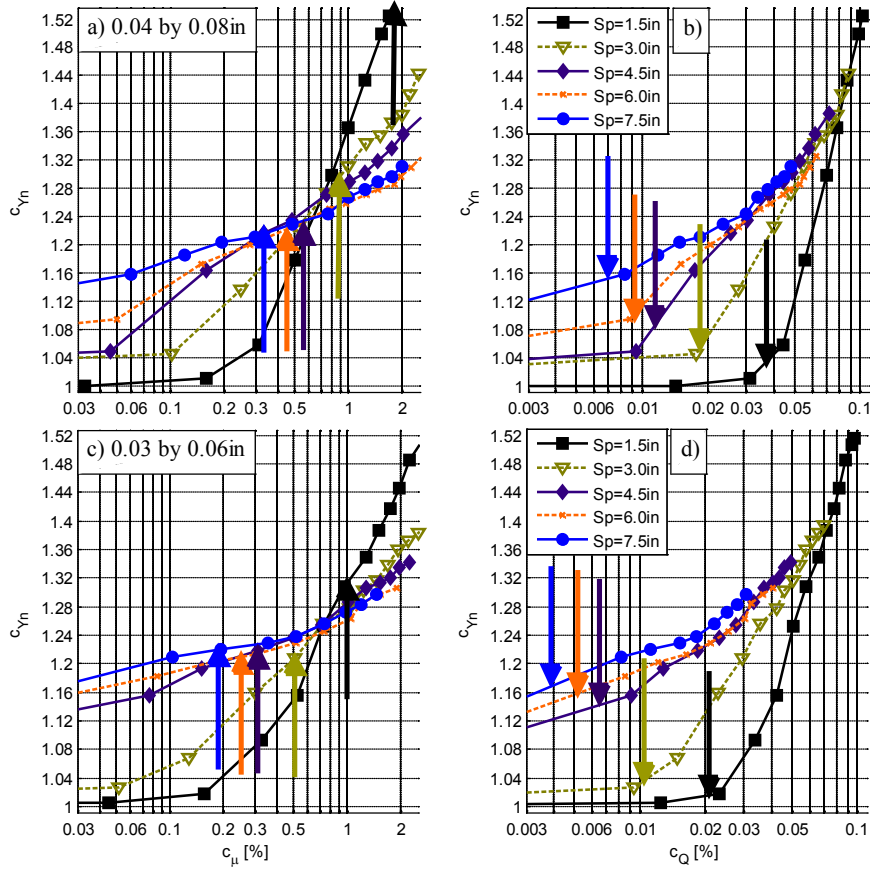
8

Fig. 10 Efficiency of different actuator spacings at δ_R=60%, β=0° and u_∞=40m/s with: a-b) 0.04 by 0.08in. actuators; c-d) 0.03 by 0.06in. actuators (arrows pointing up indicate U_j=U_c; arrows pointing down indicate U_j=3•U_∞).
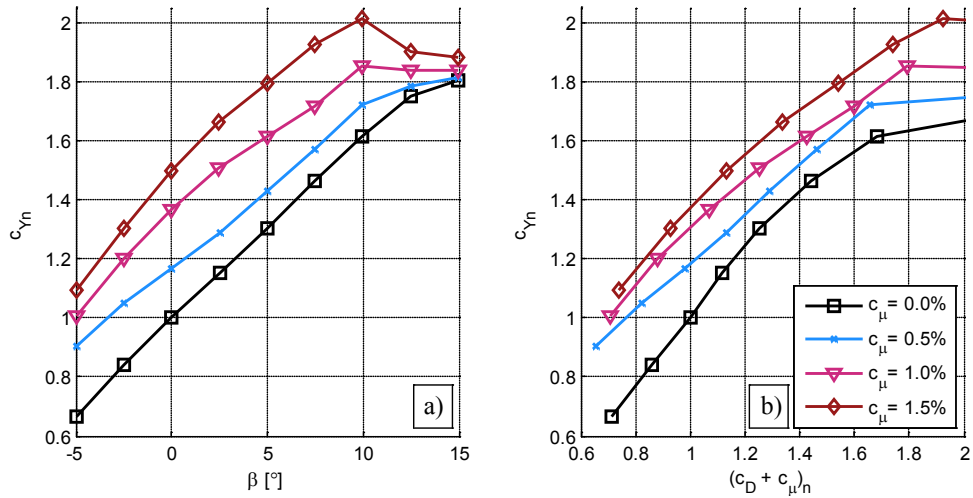

Fig. 11 The effect of side slip on lift and drag for δ_R=60% at u_∞=40m/s with 1.5in. spacing 0.04 by 0.08in. actuators.

Flying with asymmetric thrust due to a one "engine out" condition may require flying at a small side slip angle, β, even at a reduced speed and altitude. The side slip should be minimized if not eliminated when a long cruise with a single engine is anticipated (ETOPS certification). Assume that a normalized $C_{Yn}=1.2$ is required to fly "straight and level" with a single engine on the airplane shown in Fig. 1. This condition can be attained at $\delta_R=60\%$ and $\beta=3^o$ and it results in a drag penalty of 20%. Using sweeping jets at $C_\mu \approx 0.5\%$ attains the same result at $\beta \approx 0^o$ without any drag penalty even after accounting for the added momentum input (Fig. 11b). Increasing the C_μ further to 1% can reduce the drag by an additional 15%; at this δ_R but at a negative $\beta=-2.5^o$. This opens the possibility of requiring a smaller rudder deflection at cruise which lowers the drag further. The negative values of β providing the required value of C_{Yn} may be used to prevent the "Weather Vane" effect on takeoff or landing with substantial cross wind component.

When sizing a vertical tail or wing one may use figures akin to Fig. 12 where it is shown how a given C_{Yn} can be provided by a combination of δ_R, β, or C_μ. Suppose the conventional rudder ($C_\mu=0$) would not be able to provide the needed side force of $C_{Yn}=1.2$ at $\beta=0°$ even at $\delta_R=80\%$ (Fig. 12a). As a result the vertical tail has to be larger to be able to provide the necessary yaw authority. Using sweeping jet actuation, a $C_\mu=1\%$ would fulfill such a requirement at $\delta_R=50\%$ thus avoiding side slip. This can enable a reduction in size of the rudder. In case $C_{Yn}=1.3$ is required a $C_\mu=2\%$ would be needed to avoid side slip or the rudder deflection would have to be increased to $\delta_R=60\%$ if C_μ of 1% would be all that is available (Fig. 12b).

This example suggests how AFC can enable a reduction in the total size of any given wing because the desired normal force generated by such a wing can be achieved by flap deflection, incidence or AFC. For the specific case of a vertical stabilizer the goal is to reduce the overall size without losing the ability to control the airplane in critical situations. Those scenarios typically occur during takeoff or landing where side slip is imposed by outside conditions. Fig. 12 indirectly shows that the necessary yaw moment could still be provided by a smaller size of the vertical stabilizer.
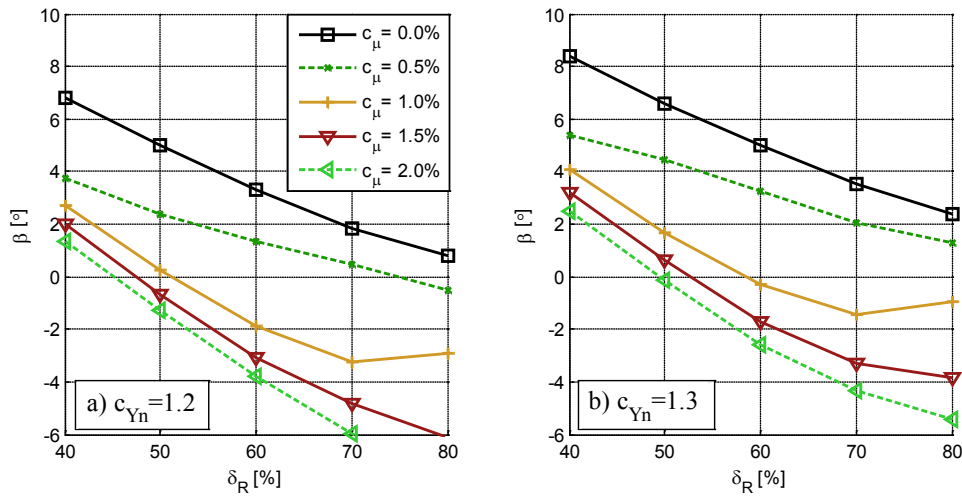

Fig. 12 Necessary rudder/side slip combination to achieve a predefined $C_{Yn}=1.2$ and 1.3, using 0.05 by 0.05in. actuators, $u_\infty=40$m/s, Sp=1.5in.

B. Some Physical Aspects of Flow Separation and its Control

Flow Visualization with tufts was used to observe the surface flow, where its direction and steadiness are of interest. In the absence of actuation the flow is separated over the rudder deflected at $\delta_R=80\%$. It is very unsteady and it is moving outward (up) along the span (Fig. 13a). Only the flow at the base of the rudder moves downward. This motion is generated by a necklace vortex created at the leading edge of the dorsal fin that is embedded in the floor boundary layer. It is further augmented by the seepage of air from the high pressure side through a gap created by the rudder deflection. Blocking the gap is impractical as it cannot be done on the airplane but when it was tried it had a deleterious effect on the side force generated by actuation.

10

Sweeping jet actuation at δ_R=80% and C_μ=2% attaches the flow over 2/3 of the span with the exception of the base region where the corner vortex persists. The tufts in the attached shoulder region are stationary and they are approximately perpendicular to the rudder hinge (Fig. 13b). In order to attach the flow over most of the span without increasing C_μ further the rudder deflection had to be reduced (Fig. 13c). Even under these circumstances there are two regions that remain dominated by large streamwise vortices. One is the tip vortex region that affects some 10% of the rudder tip region and the other is the bottom corner region discussed above. It is somewhat surprising that for evenly spaced equal size actuators insufficient C_μ results in separation approximately located at 2/3 of the tail's span. The reason for this non-uniformity is probably related to the sweep back of the tail that accumulates chordwise vorticity resulting from the spanwise boundary layer flow. This flow component also pulls vortical fluid from the floor of the tunnel (or the airplane's fuselage) upward.
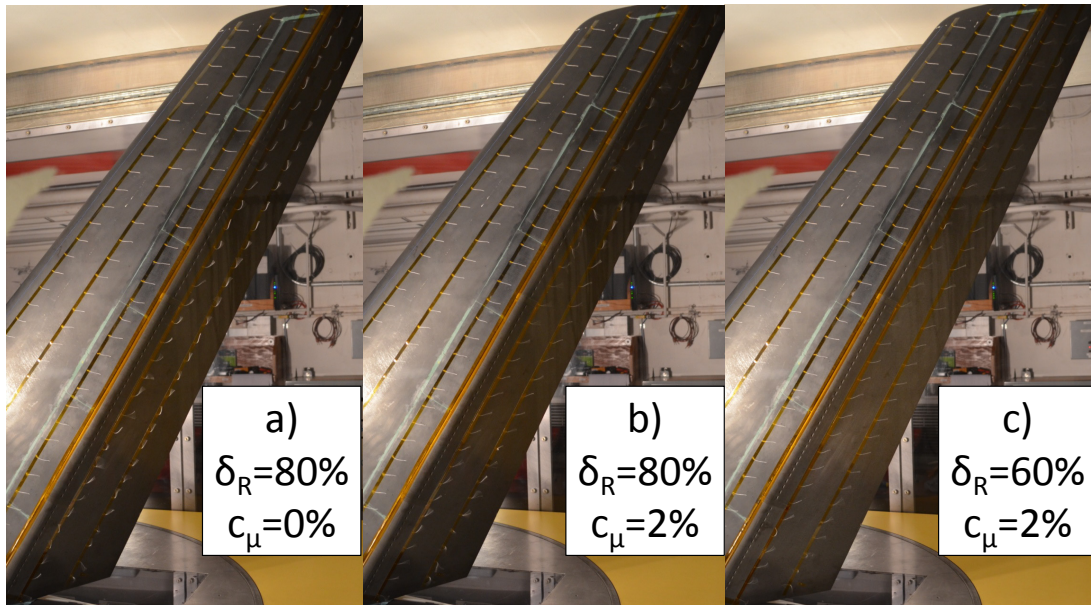

Fig. 13 Flow visualization showing attachment only in the middle lower region at δ_R=80% and complete attachment over the rudder at δ_R=60% Actuation from rudder: 0.05 by 0.05in. actuators, u_∞=30m/s, β=0° and 1.5in. spacing.
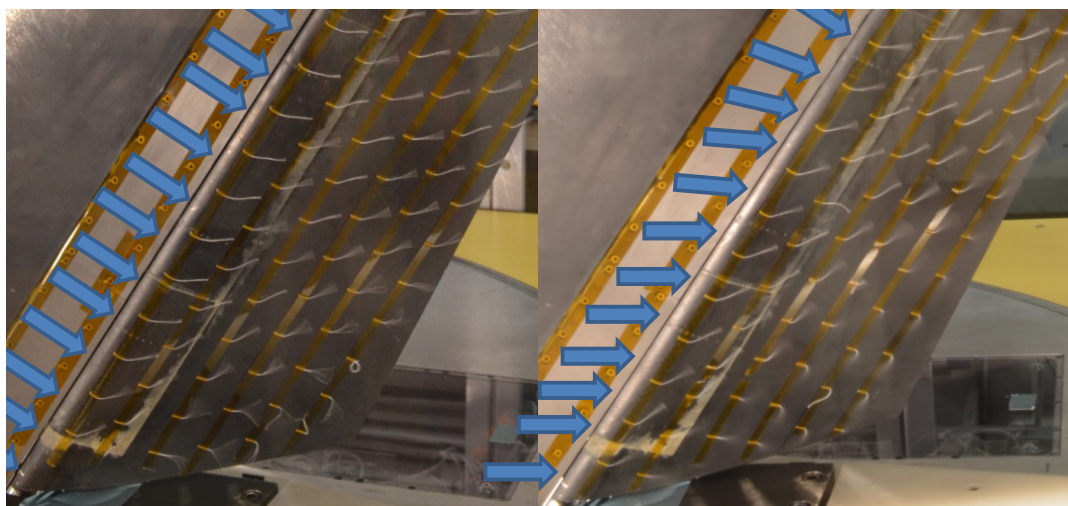

Fig. 14 The effect of actuation orientation on flow reattachment.

Since the direction of the reattached flow is approximately aligned with the free stream a question was raised about the actuation direction that was conveniently made normal to the rudder hinge. The idea of forcing normal to the leading edge came from experiments on the outer part of a swept back λ-wing [9] where the direction of actuation was first investigated. In order to verify that actuation in the direction of the free stream is indeed less efficient, a set of actuators was built that were aligned in that direction. The results were inferior relative to the original direction chosen and forced reattachment of the flow required a larger level of actuation input. A comparison of the tuft visualization near the root of the rudder at δ_R=60% and C_μ=2% is shown in Fig. 14. While the flow is mostly attached with the actuation being normal to the hinge, it remains partly separated when the actuation takes place in the direction of streaming. There was a 5% difference in the side force generated by the rudder at C_μ=1.5% with otherwise identical conditions.

The observation shown in Fig. 13b where the flow remained separated over the outer region of the rudder sparked an investigation about the wisdom of applying uniform AFC input along the span. If the streamwise tip vortex that represents a manifestation of the side force generated by the rudder cannot be controlled, one may not have to "waste" actuation on that region. A comparison of Fig. 13b and Fig. 13c suggests that the extent of the uncontrolled region depends on the level of C_μ and on the rudder deflection angle, both can be summed up by the C_{Yn} generated by the rudder with and without the application of AFC. The results plotted in Fig. 15a show the effect of methodical removal of actuators from the tip region. The ordinate represents the difference between the measured C_{Yn} with some actuators being inactive and all the actuators used at a given C_μ, while the abscissa represents the inactive tip length in percentage of span. It transpired that stopping the actuation at 85% of the span has no deleterious effect on C_{Yn} up to the highest C_μ tested in this experiment.

Removal of actuators from the root region had an immediate effect on the C_{Yn} generated by the rudder at the highest C_μ=1.7% for this configuration (Fig. 15b). If however, C_μ=1% is not exceeded at this δ_R, one could only focus the actuation on the central 65% of the span without noticing degradation in performance. The optimization of the extent at which sweeping jet actuators are effective depends on the rudder deflection as well, thus one should place limits on the combined effect of rudder deflection and C_μ on the spanwise extent in which AFC is carried out. This observation led to an investigation of regional application of AFC that was in part triggered by CFD input. [20]
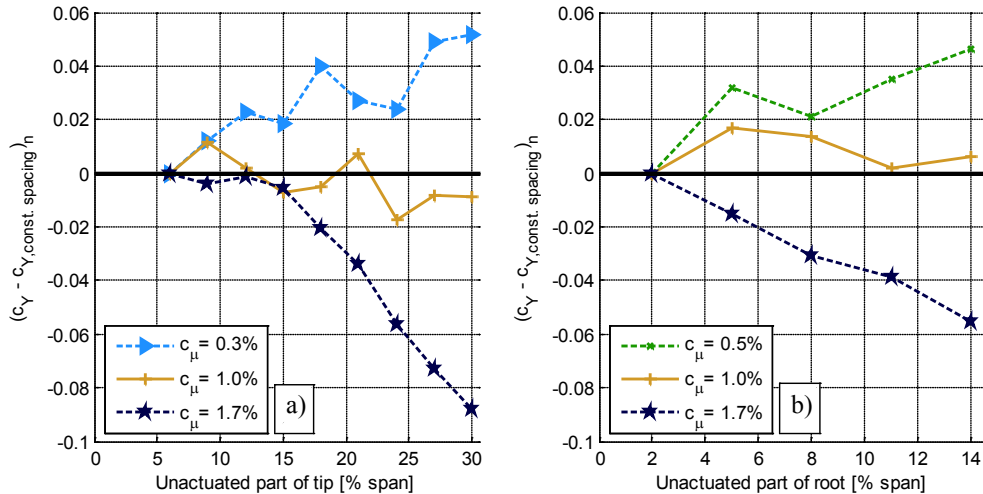

Fig. 15 Effect of removing actuation near the tip (a) or the root (b) at δ_R=60°, β=0° and u_∞=40m/s with Sp=1.5in., 0.04 by 0.08in. actuators.

Dividing the span into four equal segments and actuating from each segment separately at δ_R=60% generates the side forces shown in Fig. 16. The two central segments provide identical results irrespective of C_μ. The lowest segment (1/4span) catches up with the central two when C_μ>0.7%, suggesting that above this threshold level the effect of the corner and necklace vortices is diminished. The tip segment generates much smaller C_{Yn} than the other three confirming the previous observations. When all four segments were actuated simultaneously the C_{Yn} reached at this spacing was 1.5 at C_μ=1.5%. (Fig. 6), and when the effect

12

of all segments is summed assuming linear superposition the C_{Yn} generated should have been approximately 1.7 at the same C_μ. One may use the same number of actuators that were used in each segment but distribute them equally along the entire span. This eliminates all compressibility effects from the comparison but it requires a gap of 6 inches between adjacent actuators. The result indicates that evenly distributed actuators at large distances apart are much more effective than a concentration of actuation in a prescribed region.
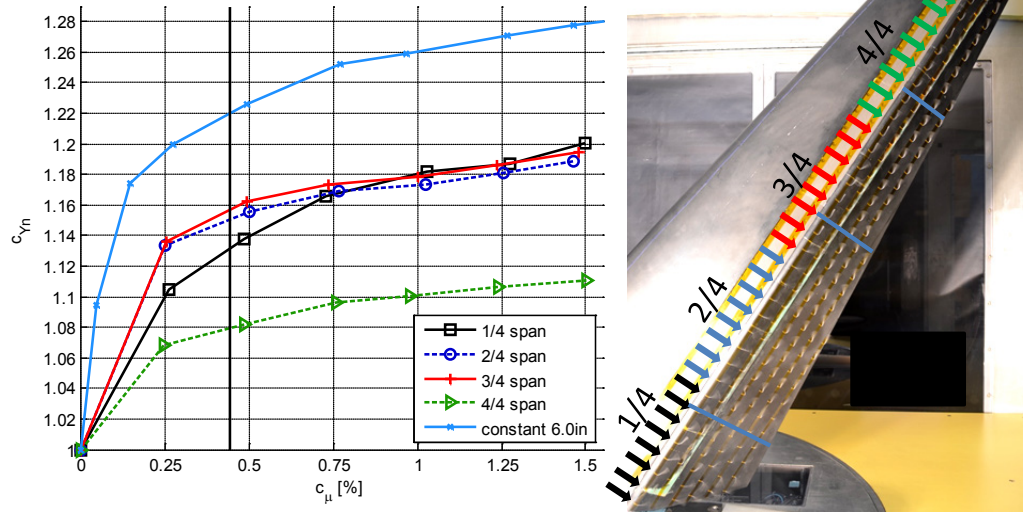

Fig. 16 The effectiveness of actuating from different spanwise sections at δ_R=60%, β=0° and u_∞=40m/s with 1.5in. spacing, 40x80 actuators (vertical line indicates (U_j=U_c)).

One may ask about the cause for the ineffectiveness of concentrated regional AFC and the best way to demonstrate this is to use one of the two central quarters. Tuft visualization is shown in Fig. 17a where δ_R=60% and the total C_μ=1.5% implying that locally there is a very large concentration of momentum. The flow over the deflected rudder directly downstream of the active sweeping jets is attached. This creates a very low pressure near the rudder hinge that generates a secondary flow toward the actuated region from both above and below its spanwise boundaries. One may clearly observe that the first row of tufts above the actuated region is pointing down (Fig. 17a), while in the absence of actuation these tufts point all up toward the tip as a result of separation (Fig. 16b). The downward entrainment effect is not local because it takes an additional 30% of the span for the tufts to revert to their separated condition. The effect on the root region is opposite since the spanwise jet entrainment pulls flow from below resulting in earlier separation and reduced side force generated by that region.

Chordwise pressure distributions (Fig. 17c) are consistent with the observations obtained by the tufts. Measurements taken at approximately 3in. (approximately 2 actuator spacings) below the lowest sweeping jet actuator indicate that the negative pressure peak at the rudder hinge decreased from C_p=-3.2 corresponding to the baseline (C_μ=0) to C_p=-2.5 for a C_μ=1.5% when AFC is concentrated at the second quarter (2/4) span. The inboard pressure distribution over the rudder suggests an existence of a streamwise vortex as it possesses a double peak. Baseline pressure distribution in the mid section that is above the actuated region suggests that the flow is completely separated over the rudder having approximately C_p=-1 at the trailing edge (Fig. 17c). The application of AFC below this line generates a C_p=-3.6 over the rudder shoulder and it reduces the pressure over the entire tail section at this spanwise location. This low pressure corresponds to the region where the tufts point downward toward the sweeping jets (Fig. 17a). The flow is probably separated over the next fraction of the rudder chord (0.7<x/c<0.8), but the pressure tap line intersects the edge of the sweeping jet at or near the trailing edge of the rudder resulting in an apparent sharp increase in pressure between 0.8<x/c<1.0. The last tuft at the edge of the actuation and the trailing edge is aligned approximately with the free stream direction and this is consistent with the C_p distribution. The flow over the rudder corresponding to the outboard pressure-tap-line is separated but the effect of

13

entrainment is felt even at this spanwise location that is roughly 16in. (approximately 10 actuator distances) above the active jets boundary (Fig. 17c).
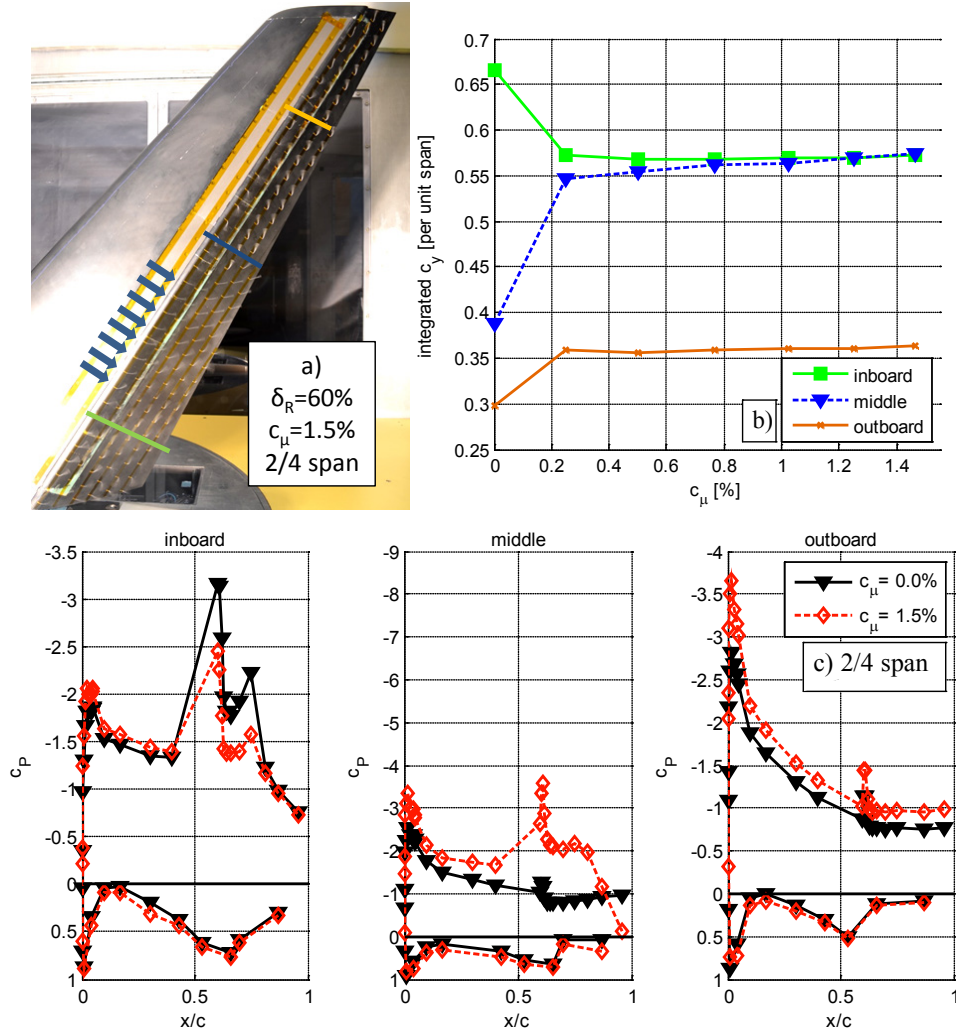

Fig. 17 Concentrating the actuation over the second quarter of the span at $\delta_R=60\%$, $C_\mu =1.5\%$ with 0.04 by 0.08in. actuators: a) tuft visualization; b) the effect of C_μ on integrated pressure; c) chordwise pressure distributions.

Integrating the pressure distribution per unit span provides an integrated side force that is assessed for the entire range of C_μ considered. The effect of the actuation in the second segment has a deleterious effect on the C_{Yn} generated by the lower section (Fig. 17b). It has a large positive effect on the second array of chordwise pressure taps ("middle section"), due to the jet entrainment that redirects some flow toward the root of the vertical tail. The effect persists toward the tip but it is much weaker there (Fig. 17b). It is interesting to note that these pressure distributions are sensitive to an increase in C_μ as long as the latter is smaller than 0.25%. This number seems deceivingly small, but it represents an overall C_μ that is concentrated over a ¼ of the span. So locally the effect seems to saturate at $C_\mu \approx 1\%$ that bodes well with the integral results achieved for uniform actuation along the span.

C. Actuation Location

Actuation on a generic uncambered but flapped airfoil [11,12] indicated that actuation from the flap is more effective than actuation from the main element of the airfoil. This is partly because separation

14

occurred on the flap and the jets helped the flow to turn around the flap shoulder. The distinction between the actuation from the flap and the main element might have been exaggerated because the jets were always inclined at 30° to the downstream upper surface thus for a flap deflected at some positive δ_R, the jet emanating from the main element was inclined relative to the downstream surface at $(\delta_R+30°)$. Thus at large flap deflection the ejection angle might have been a cause of inefficiency. This was the reason that actuation emanating from the trailing edge of the main element of the vertical tail was tangential to the upper surface in this study.
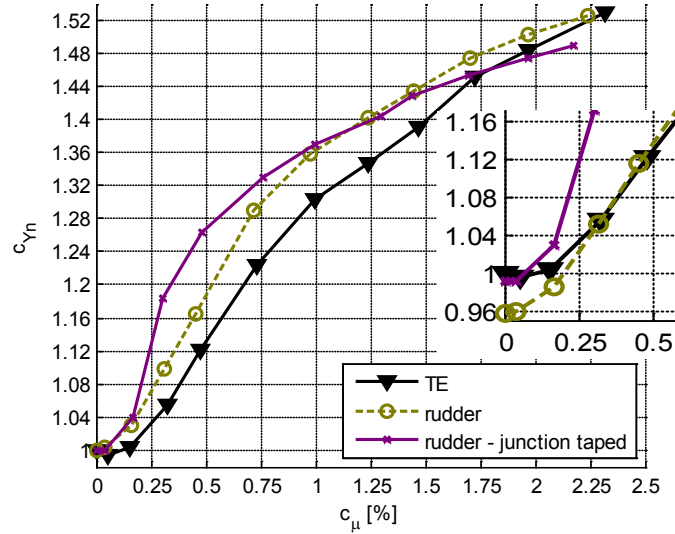

Fig. 18 The effect of C_μ on the side force generated by actuation from the rudder and from the TE of the main element. $\delta_R=60\%$, Sp =1.5in., $\beta=0^o$, actuator nozzle size: 0.05 by 0.05in.

A different rudder was built that contained an array of actuators at 5% of its chord and was installed into the vertical tail that had another array of actuators at its TE. The added roughness associated with the actuator nozzles reduced the baseline performance of the rudder by approximately 4% (see inset in Fig. 18). Since the actuators located at the TE were not used concomitantly with the rudder actuators they were taped over, resulting in a side force increase of almost 4% suggesting that this penalty is introduced by an array of idle actuators into the boundary layer flow. One may thus normalize all the values shown in Fig. 18 by their respective baseline values. For $C_\mu<1.7\%$ actuation from the rudder is superior to the actuation from the TE, particularly if the transition between the main element and the rudder is smooth. For example: at $C_\mu=0.5\%$, actuation from the rudder increased its effectiveness by 25% while actuation from the TE increased it by a mere 12% (Fig. 18). This effect became smaller at higher C_μ and at larger values of Sp.

The differences between TE actuation and rudder actuation all but disappeared when Sp was doubled or quadrupled. Nevertheless, a strong coupling among many of the parameters affecting the flow exists. It proves once again that although C_μ is perhaps the most important parameter governing the flow it is not the sole parameter affecting it. In the picture below (Fig. 19) the two actuation locations were compared at $\delta_R=80\%$. On the right hand side (RHS) the actuators were located at the TE and spaced 3in. apart while on the left hand side (LHS) they were on the flap and spaced at 1.5in.. The flow on the left is attached over 75% of the rudder while the flow on the right is almost entirely separated in spite of the lower C_μ used on the LHS. The volume flow of air is almost equal in both cases because of the different distance between adjacent actuators. These pictures illustrate the complexity of this multi parameter problem that requires careful optimization based on a good understanding of the flow physics. Nevertheless even a suboptimal application of the active separation control may provide between 30% and 40% improvement in the side force generated by the vertical tail.
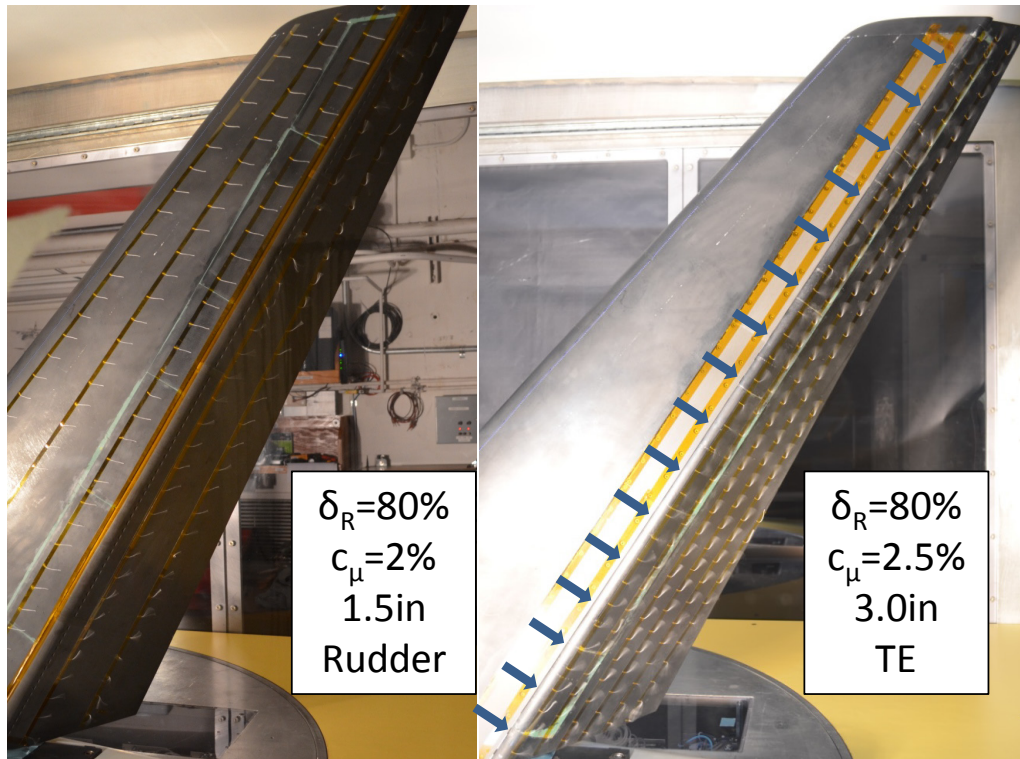
15

Fig. 19 The effect of different actuation locations and spacing on the flow over a rudder.

IV.   Outlook and Conclusions

The size of the vertical tail on a multi engine airplane is determined by the eventuality of engine loss after takeoff and during climb. It is a large surface that has to provide adequate yaw control during "engine out" emergency. Normal rudder operations, even during cross-wind takeoff or landing are much less demanding. Thus an increase in rudder efficiency can reduce the drag and weight of a prospective airplane. The vertical tail is a good proving ground for nascent high lift technologies since its maximum lift capabilities are not required for all but a few emergency situations. If the total size of the vertical stabilizer is decreased while the necessary yaw authority for those few critical scenarios is still maintained by AFC, an added benefit for the entire flight envelope may be achieved.

This report describes experiments carried out on a typical vertical tail of a commercial airplane in order to increase the effectiveness of its rudder. The use of sweeping jets placed on the surface close to the rudder hinge improved the control authority of the rudder by approximately 50% at reasonable mass flow or momentum coefficients. Although the task of designing the actuators and their integration into the system is incomplete, there are a few pointers worth mentioning:

1. Most of the benefits are reaped out at $C_\mu < 1\%$
2. The size of the actuators and the distance measured between adjacent ones determines the effectiveness of the system.
3. Jet velocities should be at least 3 times larger than the free stream but they should remain subsonic for most effective actuation.
4. Actuation from the rudder is more effective provided all other factors are identical.
5. The average jet axis emanating from actuators should be perpendicular to the leading edge and if this is not practical, the jet axis should be normal to the rudder hinge.
6. Distributing actuation evenly (even at large distances apart) is much more effective than concentrating it in a prescribed region.

7. Separate investigations have shown that the total aspect ratio (most importantly of the surface orifice dimensions) should not exceed 2.
8. There generally is a strong coupling among all the tools used to generate large side force on a given vertical tail (e.g. rudder deflection, C_μ, actuator size, aspect ratio, spacing and location).

The large increase in rudder effectiveness provides an opportunity for a fresh airplane design where yaw control is provided by winglets instead of a separate vertical stabilizer (see Fig. 20). In this case the "rudder" may actually contribute to drag reduction.
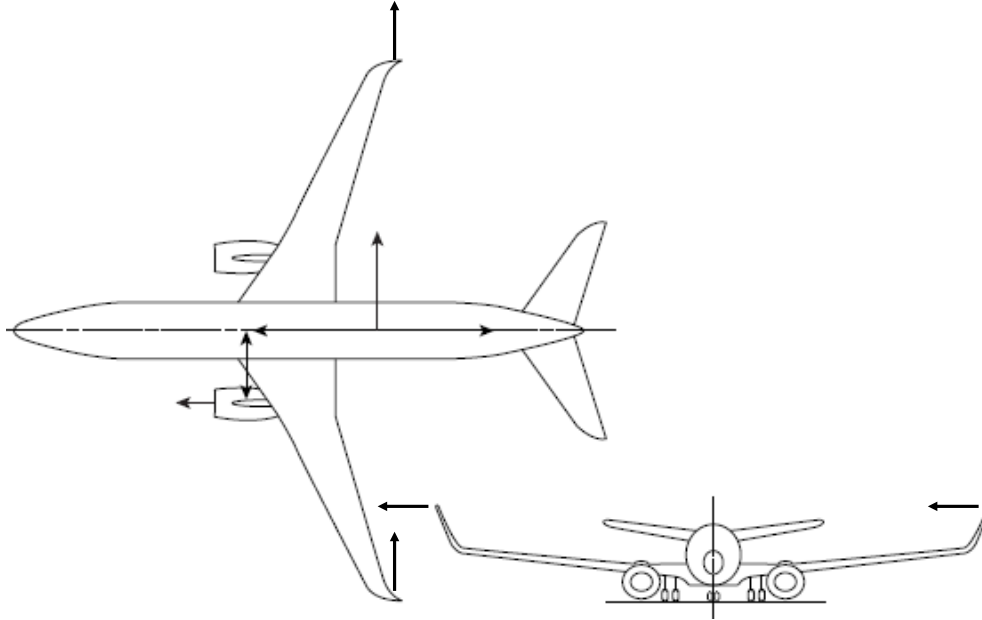

Fig. 20 Airplane design featuring yaw control through winglets

Acknowledgments

References

[1] Cattafesta III, L.N. and Sheplak, M., "Actuators for Active Flow Control", *Annual Review of Fluid Mechanics*, doi: 10.1146/annurev-fluid-122109-160634, Vol. 43, Issue 1, Aug. 2010, pp. 247-272.

[2] Guyot, D., Bobusch, B., Paschereit, C.O., and Raghu, S., "Active Combustion Control Using a Fluidic Oscillator for Asymmetric Fuel Flow Modulation", *AIAA 2008-4956, 44th AIAA/ASME/SAE/ASEE Joint Propulsion Conference & Exhibit*, Hartford, CT, July 2008.

[3] Cerretelli, C., Gharaibah, E., Toplack, G., Gupta, A., and Wuerz, W., "Unsteady Separation Control for Wind Turbine Applications at Full Scale Reynolds Numbers", *AIAA 2009-380, 47th AIAA Aerospace Science Meeting*, Orlando, FL, Jan. 2009.

[4] Cerretelli, C. and Kirtley, K., "Boundary Layer Separation Control with Fluidic Oscillators", *Journal of Turbomachinery*, doi: 10.1115/1.3066242, Vol. 131, Oct. 2009.

[5] Lucas, N., Taubert, L., Woszidlo, R., Wygnanski, I., and McVeigh, M. A., "Discrete Sweeping Jets as Tools for Separation Control," 4th Flow Control Conference, Seattle, WA, AIAA 2008-3868, June 23-26, 2008.

[6] Seele, R., Tewes, P., Woszidlo, R., McVeigh, M., Lucas, N., and Wygnanski, I., "Discrete Sweeping Jets as Tools for Improving the Performance of the V-22", *AIAA Journal of Aircraft*, doi: 10.2514/1.43663, Vol. 46, No. 6, 2009, pp. 2098-2106.

17

[7] Phillips, E., Woszidlo, R., and Wygnanski, J., "The Dynamics of Separation Control on a Rapidly Actuated Flap", *AIAA 2010-4246, AIAA 5th Flow Control Conference*, 28 June-1 July, Chicago, IL, 2010.

[8] DeSalvo, M., Whalen, E., and Glezer, A., "High-Lift Enhancement Using Active Flow Control", *AIAA 2011-3355, AIAA 29th Applied Aerodynamics Conference*, 27-30 June, Honolulu, HI, 2011.

[9] Tewes, P., Taubert, L., and Wygnanski, J., "On the Use of Sweeping Jets to Augment the Lift of a λ-Wing", *AIAA 2010-4689, AIAA 5th Flow Control Conference*, 28 June-1 July, Chicago, IL, 2010.

[10] Vatsa, V., Koklu, M and Wygnanski, I., "Numerical Simulation of Fluidic Actuators for Flow Control Applications", *AIAA-2012-3239, AIAA 6th Flow Control Conference*, 26 – 29 June, New Orleans, LA, 2012.

[11] Woszidlo, R. and Wygnanski, I., "Parameters Governing Separation Control with Sweeping Jet Actuators", *AIAA 2011-3172, AIAA 29th Applied Aerodynamics Conference*, 27-30 June, Honolulu, HI, 2011.

[12] Woszidlo, R., Nawroth, H., Raghu, S., and Wygnanski, I., "Parametric Study of Sweeping Jet Actuators for Separation Control", *AIAA 2010-4247, AIAA 5th Flow Control Conference*, 28 June – 1 July, Chicago, Illinois, 2010.

[13] Raman, G. and Raghu, S., "Cavity Resonance Suppression Using Miniature Fluidic Oscillators", *AIAA Journal*, doi:10.2514/1.521, Vol. 42, No. 12, Dec. 2004, pp. 2608-2611.

[14] Rathay, N., Boucher, M., Amitay, M. and Whalen, E., "Performance Enhancement of a Vertical Stabilizer using Synthetic Jet Actuators: No Sideslip", *AIAA 2012-0071, AIAA 50th Aerospace Sciences Meeting*, 09-12 January, Nashville, TN, 2012.

[15] Rathay, N., Boucher, M., Amitay, M. and Whalen, E., "Performance Enhancement of a Vertical Stabilizer using Synthetic Jet Actuators: Non-zero Sideslip", *AIAA 2012-2657, 6th AIAA Flow Control Conference 25 - 28 June*, New Orleans, LA, 2012

[16] Seele, R., Graff, E., Gharib, M., Taubert, L., Lin, J. and Wygnanski, I., "Improving Rudder Effectiveness with Sweeping Jet Actuators", *AIAA paper 2012-3244, presented at 6th AIAA Flow Control Conference, 25 - 28 June*, New Orleans, LA, 2012

[17] for more information: http://windtunnel.caltech.edu/

[18] Raman, G., Hailye, M. and Rice, E.J., "Flip-Flop Jet Nozzle Extended to Supersonic Flows", *AIAA Journal*, doi: 10.2514/3.11725, Vol. 31, No. 6, June 1993, pp. 1028-1035.

[19] Chen, C., Seele, R., Wygnanski, I., "Separation and Circulation Control on an Elliptical Airfoil by Steady Blowing", AIAA Journal, Vol. 50, No.10, pp. 2235-2247, October 2012

[20] Private communication with Arvin Shmilovich